MATERIALE PLASTICE
https://revmaterialeplastice.ro
https://doi.org/10.37358/Mat.Plast.1964

Construction of a Gelatin Methacryloyl and Sodium Alginate Double-Network Hydrogel for a Three-Dimensional Thyroid Cancer Cell Invasion Model

XIAO FENG, XIAOHONG XU, WENQI TANG*
Nursing Department, Shanghai Jiao Tong University School of Medicine Affiliated Sixth People's Hospital, Shanghai, China

Abstract: ***Background:*** *Thyroid cancer remains the most common endocrine malignancy, and a subset of patients exhibit aggressive invasion and recurrence. Conventional two-dimensional culture models fail to replicate the three-dimensional (3D) tumor microenvironment, underscoring the need for biomimetic scaffolds to study invasion and therapy response.* ***Methods:*** *GelMA/SA double-network hydrogels with different ratios (3:1, 1:1, 1:3) were fabricated by sequential photocrosslinking and ionic crosslinking. Their swelling, degradation, and mechanical properties were characterized, and microstructures were examined by scanning electron microscopy. Human papillary thyroid carcinoma cell lines (TPC-1 and BCPAP) were encapsulated to evaluate viability, morphology, and invasive behavior.* ***Results:*** *The hydrogel composition strongly influenced structural and biological performance. SA-rich gels showed excessive swelling, rapid degradation, and poor pore formation, while GelMA-rich gels were stable but less porous. The intermediate 1:1 formulation exhibited balanced swelling and degradation, uniform pores, and enhanced tensile and compressive strength. Encapsulated cells in the 1:1 gels displayed robust viability, extended pseudopodia, and maintained expression of invasion-related markers (N-cadherin, MMP-9).* ***Conclusion:*** *The GelMA: SA = 1:1 double-network hydrogel provides the most favorable microenvironment for thyroid cancer cell invasion modeling, combining porosity, stability, and bioactivity. This 3D platform offers a reliable tool for mechanistic studies and therapeutic evaluation in thyroid cancer.*

Keywords: *Thyroid cancer, GelMA/alginate hydrogel, double-network hydrogel, three-dimensional culture, invasion model, TPC-1 cells, BCPAP cells, extracellular matrix*

1. Introduction

Thyroid cancer is the most common malignancy of the endocrine system, with papillary thyroid carcinoma representing the predominant subtype [1–3]. Although the majority of patients have favorable outcomes after surgery and radioiodine therapy, a subset of cases exhibit aggressive local invasion and recurrence, which poses a major clinical challenge [4,5]. To elucidate the mechanisms of invasion and evaluate novel therapeutic approaches, *in vitro* models that accurately mimic the tumor microenvironment are required [6–8]. Conventional two-dimensional (2D) culture systems, however, fail to capture the spatial organization, extracellular matrix (ECM) cues, and biochemical gradients that influence tumor progression *in vivo*, resulting in discrepancies between *in vitro* observations and patient pathology [9]. This limitation has driven increasing interest in the development of three-dimensional (3D) culture models for cancer research [10,11].

Hydrogels are widely employed as 3D scaffolds due to their high water content, tunable mechanical properties, and structural similarity to native ECM [12,13]. Gelatin methacryloyl (GelMA) provides bioactive motifs that facilitate cell attachment and spreading, but its networks are mechanically weak and prone to collapse during long-term culture [14,15]. Sodium alginate (SA), in contrast, readily forms ionically crosslinked networks with calcium ions, conferring good mechanical stability but lacking

email: 18930177049@189.cn

intrinsic cell adhesion sites, rendering it biologically inert [16,17]. To overcome the limitations of single-component systems, hybrid DN hydrogels (DN-hydrogels) composed of GelMA and SA have been proposed [18]. This design integrates GelMA's bioactivity with SA's structural reinforcement, potentially achieving a more physiologically relevant balance of porosity, stability, and biofunctionality [19]. However, the impact of different GelMA/SA ratios on microstructure, mechanical strength, and their ability to support thyroid cancer cell invasion remains largely unexplored [8,20].

In this study, GelMA/SA DN DN hydrogels with ratios of 3:1, 1:1, and 1:3 were fabricated and systematically evaluated. Their swelling, degradation, and mechanical properties were characterized, and morphological differences were examined by scanning electron microscopy. Human papillary thyroid carcinoma cell lines (TPC-1 and BCPAP) were encapsulated within these hydrogels to assess cell viability, cytoskeletal organization, and invasive potential, including the expression of invasion-related genes such as N-cadherin and MMP-9. We hypothesized that the intermediate 1:1 composition would provide the most favorable microenvironment, combining sufficient porosity and mechanical stability with appropriate bioactivity to sustain cell proliferation and invasion. This work establishes a biomimetic 3D thyroid cancer invasion model and provides a foundation for future applications in mechanistic studies, drug screening, and personalized therapeutic strategies.

2. Materials and methods

2.1. Materials

Gelatin methacryloyl (GelMA, degree of substitution ~80%) was purchased from EFL Biotechnology, Suzhou, China (Cat. No. GM-80). Sodium alginate (medium viscosity, from brown algae) was obtained from Sigma-Aldrich, St. Louis, MO, USA (Cat. No. A2033). Calcium chloride dihydrate ($CaCl_2 \cdot 2H_2O$, analytical grade) was purchased from Sinopharm Chemical Reagent Co., Ltd., Shanghai, China (Cat. No. 10017318). Lithium phenyl-2,4,6-trimethylbenzoylphosphinate (LAP) photoinitiator was purchased from Aladdin Biochemical Technology Co., Ltd., Shanghai, China (Cat. No. L174853). Dulbecco's Modified Eagle's Medium (DMEM), fetal bovine serum (FBS), and penicillin–streptomycin (P/S) were obtained from Gibco, Thermo Fisher Scientific, Waltham, MA, USA. TRIzol reagent for RNA extraction was purchased from Invitrogen, Thermo Fisher Scientific, USA. The CCK-8 cell viability kit was purchased from Dojindo Laboratories, Kumamoto, Japan (Cat. No. CK04). Antibodies for immunofluorescence, including anti-F-actin (Phalloidin-iFluor 594, Cat. No. ab176757) and DAPI nuclear stain (Cat. No. ab228549), were purchased from Abcam, Cambridge, UK. qPCR reagents (PrimeScript RT reagent kit, SYBR Premix Ex Taq II) were obtained from Takara Bio, Shiga, Japan. All reagents were used without further purification.

Human papillary thyroid carcinoma cell lines TPC-1 and BCPAP were purchased from the Cell Bank of the Chinese Academy of Sciences, Shanghai, China. Cells were authenticated by STR profiling and tested free of mycoplasma contamination prior to experiments.

2.2. Methods

2.2.1 Preparation of hydrogels

GelMA (5% w/v) was dissolved in PBS at 60°C and mixed with LAP photoinitiator (0.25% w/v). Sodium alginate (1.5% w/v) was dissolved in PBS at room temperature. To prepare DN DN hydrogels, GelMA and SA precursor solutions were mixed at defined weight ratios (GelMA:SA = 3:1, 1:1, or 1:3). The mixture was pipetted into custom cylindrical molds (diameter 6 mm, height 2 mm). GelMA was photocrosslinked under 405 nm light (10 mW/cm^2, 60 s), followed by immersion in 100 mM $CaCl_2$ solution for 30 min to achieve SA ionic crosslinking. Single GelMA or SA hydrogels were prepared in parallel as controls.

2.2.2 Swelling and degradation assays

For swelling tests, hydrogels ($n = 3$ per group) were lyophilized, weighed (Wd), and immersed in PBS at 37°C. At predetermined time points (1, 3, 6, 12, and 24 h), samples were blotted and weighed (Ws). Swelling ratio was calculated as (Ws–Wd)/Wd.

For degradation tests, hydrogels were incubated in PBS (37°C) for 24 h. Samples were collected, lyophilized, and weighed (Wt). Remaining mass ratio was determined as Wt/W0, where W0 is the initial dry weight.

2.2.3 Mechanical testing

Tensile and compressive properties were tested using a universal testing machine (Instron 5943, Norwood, MA, USA) at room temperature. For tensile testing, dumbbell-shaped hydrogel samples (length 15 mm, width 5 mm, thickness 2 mm) were stretched at 5 mm/min until failure. For compression testing, cylindrical hydrogels (diameter 8 mm, height 6 mm) were compressed at 1 mm/min up to 80% strain. Stress–strain curves were recorded, and maximum stress values were calculated. All mechanical tests were performed using the GelMA:SA = 1:1 DN DN hydrogel compared with single GelMA and SA hydrogels.

2.2.4 Scanning electron microscopy (SEM)

Hydrogels were frozen at −80°C, lyophilized, and fractured to expose cross-sections. Samples were sputter-coated with gold and imaged using a Hitachi SU8020 SEM (Tokyo, Japan) at 5 kV. Pore morphology, pore size distribution, and wall thickness were analyzed qualitatively.

2.2.5 Cell culture and encapsulation

TPC-1 and BCPAP cells were cultured in DMEM supplemented with 10% FBS and 1% P/S in a humidified incubator at 37°C with 5% CO_2. For encapsulation, cell suspensions (1×10^6 cells/mL) were mixed with precursor GelMA/SA solutions before crosslinking. Constructs were cultured in 24-well plates, and medium was refreshed every 2 days.

2.2.6 Confocal immunofluorescence

Cells encapsulated in hydrogels were fixed with 4% paraformaldehyde (15 min), permeabilized with 0.1% Triton X-100 (10 min), and blocked with 5% BSA (1 h). Samples were stained with Phalloidin-iFluor 594 (1:200, 1 h) and counterstained with DAPI (1 μg/mL, 5 min). Images were acquired with a Leica TCS SP8 confocal microscope (Wetzlar, Germany) using 40× oil immersion objectives.

2.2.7 Cell viability assay (CCK-8)

Cell viability was evaluated at days 0, 1, 2, and 3. Hydrogels were incubated in 10% CCK-8 solution (v/v in DMEM) for 2 h at 37°C. Supernatants were transferred to 96-well plates, and absorbance was measured at 450 nm using a microplate reader (BioTek Synergy H1, Winooski, VT, USA). Results were normalized to day 0.

2.2.8 qPCR analysis

After 3 days of culture, total RNA was extracted from hydrogels using TRIzol reagent following manufacturer's protocol. RNA concentration and purity were assessed by NanoDrop 2000 spectrophotometer (Thermo Fisher, USA). Reverse transcription was carried out using the PrimeScript RT reagent kit. qPCR was performed with SYBR Premix Ex Taq II on a LightCycler 480 system (Roche, Switzerland). Primers were as follows:

N-cadherin (CDH2): F-5′-AGGCTTCTGGTGAAATGGAA-3′, R-5′-TGCAGTTGCTAAACTTG CTG-3′

MMP-9: F-5′-TGTACCGCTATGGTTACACTCG-3′, R-5′-GGCAGGGACAGTTGCTTCT-3′

GAPDH: F-5′-GGAGCGAGATCCCTCCAAAAT-3′, R-5′-GGCTGTTGTCATACTTCTCATGG-3′

Relative expression was calculated by the ΔΔCt method normalized to GAPDH.

2.2.9 Statistical analysis

All quantitative data are presented as mean ± standard deviation (SD). Unless otherwise specified, each experimental condition was repeated independently at least three times ($n = 3$). For comparisons among the three hydrogel formulations (GelMA:SA = 3:1, 1:1, and 1:3), one-way analysis of variance (ANOVA) followed by Tukey's post hoc test was performed. For pairwise comparisons between two groups, an unpaired two-tailed Student's *t*-test was used. Statistical analyses were carried out using GraphPad Prism (GraphPad Software, San Diego, CA, USA). A p value < 0.05 was considered statistically significant ($^*p < 0.05$, $^{**}p < 0.01$).

3. Results

As shown in Figure 1, the designed GelMA/Calcium Alginate DN DN hydrogel was successfully prepared by sequential photocrosslinking of GelMA and ionic crosslinking of sodium alginate with calcium ions. The incorporation of thyroid cancer cells (TPC-1/BCPAP) into the hydrogel matrix resulted in a stable 3D construct with well-distributed cells throughout the scaffold. The presence of interconnected pores was evident, providing a structural framework that facilitated nutrient and oxygen diffusion, thereby supporting long-term cell survival. Compared with conventional two-dimensional cultures, the 3D hydrogel system established here provided a spatial environment that more closely resembled the *in vivo* tumor niche. Importantly, the obtained 3D constructs remained structurally stable under culture conditions, indicating that the dual-network design imparted both mechanical robustness and biocompatibility.

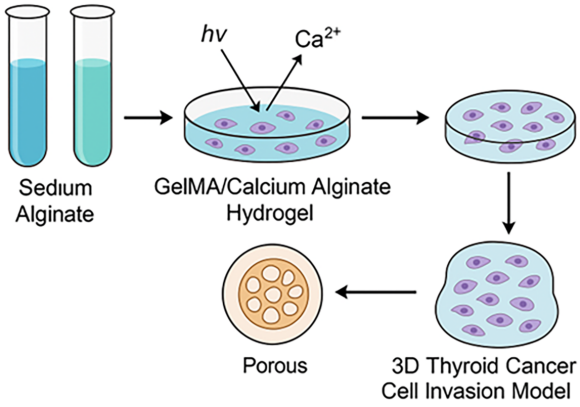

Figure 1. Schematic illustration of the preparation of GelMA/Calcium Alginate DN hydrogel and its application in constructing a 3D thyroid cancer cell invasion model. Sodium alginate and GelMA were combined, followed by photocrosslinking and Ca^{2+} ionic crosslinking to form a porous DN hydrogel that encapsulated thyroid cancer cells, thereby mimicking the extracellular environment for invasion studies

As shown in Figure 2A, the swelling behavior of the hydrogels was clearly influenced by the GelMA/SA ratio. Hydrogels with higher SA content (GelMA:SA = 1:3) exhibited the largest swelling, reaching nearly threefold within 24 h, while the GelMA-rich group (3:1) swelled only modestly, stabilizing around 2.0. The 1:1 group demonstrated intermediate and balanced swelling behavior, with a final swelling ratio of approximately 2.5. Figure 2B further shows that the degradation rates were composition-dependent: the 1:3 gels degraded fastest, retaining only ~60% of their mass at 24 h, whereas the 3:1 gels maintained over 85% of their initial weight. The 1:1 group again fell between these extremes, retaining about 70% of its weight, suggesting moderate stability. Mechanical testing was then performed specifically on the 1:1 GelMA/SA DN hydrogel. As shown in Figure 2C, its tensile stress–strain curve revealed a marked enhancement in mechanical strength, with stress values surpassing 500 kPa at 70%

strain, significantly higher than those of single GelMA or SA gels. Similarly, Figure 2D illustrates the compressive behavior of the 1:1 DN hydrogel, which reached over 300 kPa, again outperforming the single-component hydrogels that remained below 250 kPa. Together, these results indicate that the 1:1 composition provides both balanced swelling/degradation and superior mechanical reinforcement.

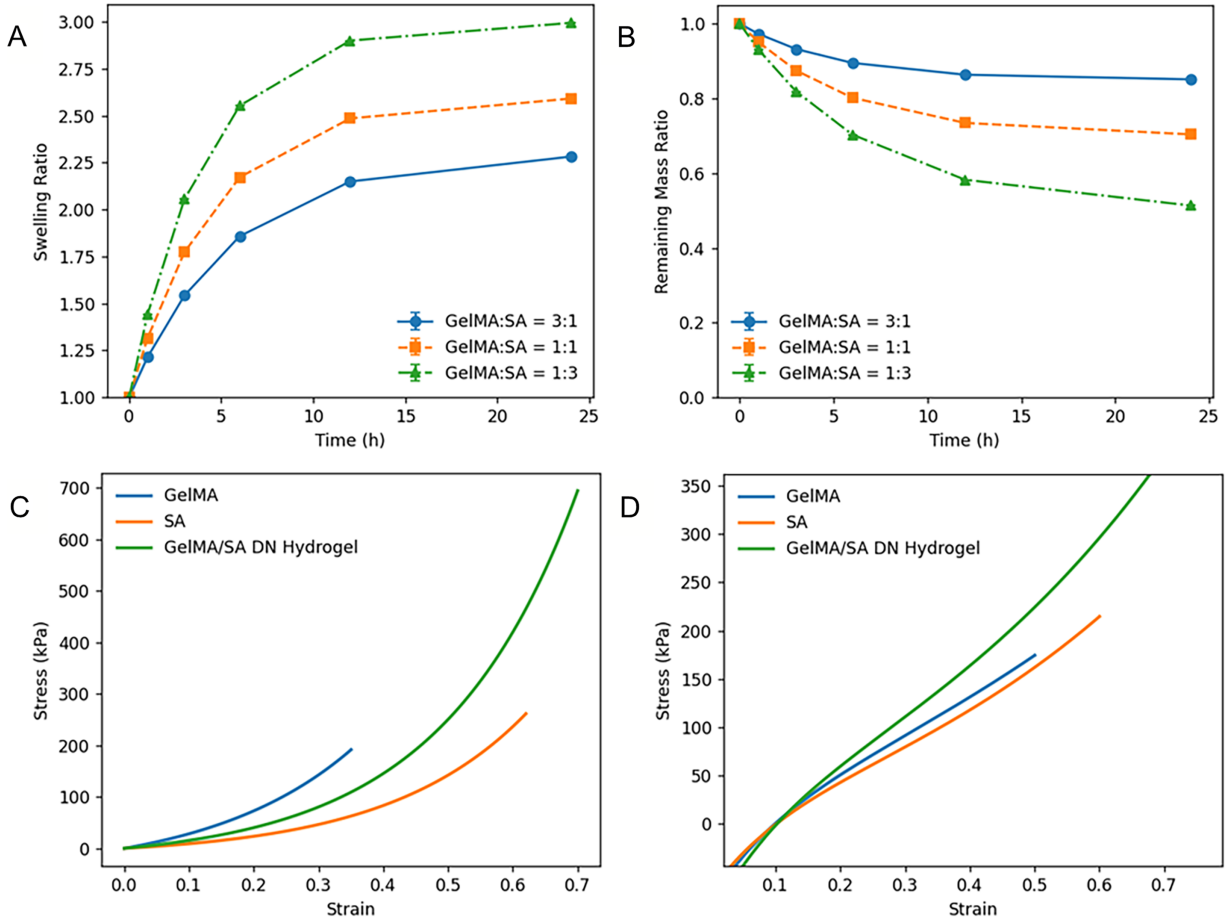

Figure 2. Characterization of GelMA/SA hydrogels with different compositions. (A) Swelling ratio of hydrogels with GelMA:SA = 3:1, 1:1, and 1:3 over 24 h. (B) Degradation profiles represented by the remaining mass ratio of the hydrogels during incubation. (C) Tensile stress–strain curves of GelMA, SA, and GelMA/SA DN hydrogels. (D) Compressive stress–strain curves of GelMA, SA, and GelMA/SA DN hydrogels

As shown in Figure 3, the three types of hydrogels displayed markedly different internal architectures depending on their composition. In the SA hydrogel (Figure 3A), the SEM image revealed a relatively dense and featureless morphology with only faint depressions rather than well-defined pores. This can be attributed to the intrinsic softness of the SA network and its reliance on reversible ionic crosslinks, which are prone to collapse during lyophilization and SEM preparation, resulting in the disappearance of stable pores. In contrast, the GelMA hydrogel (Figure 3B) exhibited a more pronounced porous structure, with larger and interconnected voids visible throughout the matrix. However, the pore walls in this group appeared thin and somewhat fragile, suggesting that although covalent photocrosslinking provided an open framework, the network lacked reinforcement and could deform under mechanical stress. Most notably, the GelMA:SA = 1:1 DN hydrogel (Figure 3C) showed a well-developed and uniformly distributed porous structure, characterized by rounded pores of relatively consistent size and thicker pore walls. The presence of both covalent GelMA chains and ionic SA crosslinks appears to have

generated a synergistic architecture that prevented collapse during drying and preserved a regular pore distribution. Collectively, these observations confirm that the DN design produces the most structurally stable and biologically favorable microenvironment. The pore architecture of the three hydrogels was further evaluated by quantitative image analysis of the SEM micrographs using ImageJ. For each formulation, at least five randomly selected fields from three independent samples were analyzed ($n = 5$ fields per sample). In the SA hydrogels, only few small, shallow depressions could be identified, yielding an apparent equivalent pore diameter of 8.4 ± 3.2 μm and an apparent porosity below 10%, consistent with the visually collapsed and compact morphology. In contrast, GelMA hydrogels exhibited a well-developed porous structure with interconnected voids; the equivalent pore diameter was 61.7 ± 19.5 μm and the pore area fraction reached 44.3 ± 7.8%. The GelMA:SA = 1:1 DN hydrogels showed the highest level of structural regularity, with pores of comparable size (72.9 ± 15.1 μm) and a significantly higher pore area fraction of 55.6 ± 6.9% compared with the single-component hydrogels ($p < 0.05$). These results confirm that the DN formulation generates a more open and homogeneous pore network, in agreement with its superior swelling and mechanical performance.

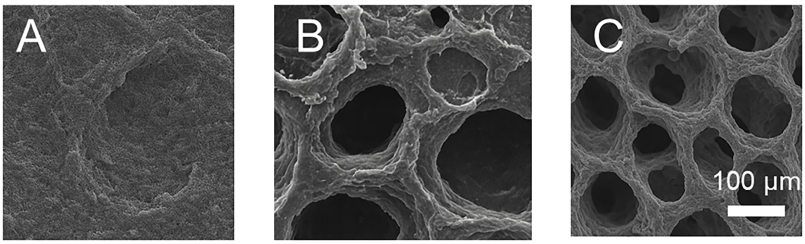

Figure 3. Representative scanning electron microscopy (SEM) images of hydrogel microstructures. (A) SA hydrogel, (B) GelMA hydrogel, and (C) GelMA:SA = 1:1 DN hydrogel. Scale bar = 100 μm

As shown in Figure 4A, confocal microscopy revealed that thyroid cancer cells encapsulated within the GelMA:SA = 1:1 hydrogel displayed a well-spread morphology with extended cytoskeletal filaments and visible pseudopodia, indicating strong cell–matrix interactions. In contrast, cells in high-SA matrices were more rounded with fewer protrusions (data not shown), consistent with a less supportive environment. Cell viability assays (Figure 4B) further confirmed that hydrogel composition directly influenced cellular proliferation. Over the 3-day culture, cells in the 1:1 group showed steady and robust growth, reaching OD450 values above 0.9, which was lower than the GelMA-rich 3:1 group but significantly higher than the SA-rich 1:3 group. The 3:1 gels supported the highest proliferation but exhibited reduced cell spreading in morphology, while the 1:3 gels restricted both viability and growth, stabilizing at OD450 around 0.6. Gene expression analysis (Figure 4C) showed that cells in the 1:1 gels exhibited balanced expression of invasion-associated markers. N-cadherin and MMP-9 were moderately expressed, whereas cells in 1:3 gels displayed marked downregulation of both markers, and cells in 3:1 gels maintained expression levels comparable to the 1:1 condition. Statistical analysis indicated that the differences between 1:1 and 1:3 groups were significant ($p < 0.01$), while the differences between 1:1 and 3:1 were not significant.

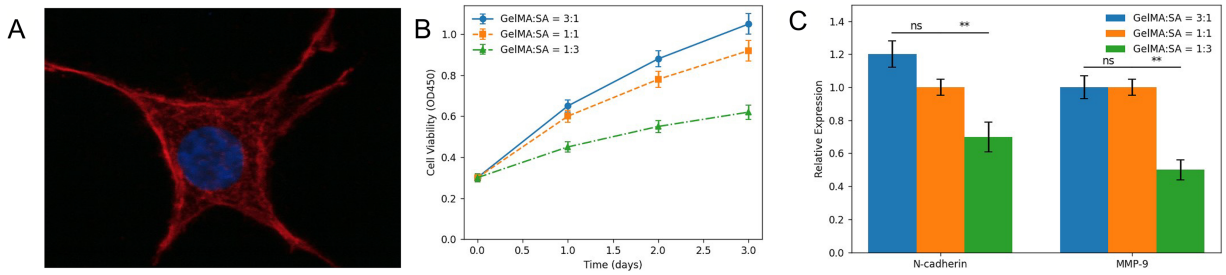

Figure 4. Biological performance of thyroid cancer cells cultured in GelMA/SA hydrogels with different compositions. (A) Representative confocal image showing a thyroid cancer cell encapsulated in the GelMA:SA = 1:1 hydrogel, stained for F-actin (red) and nuclei (blue), revealing extended morphology and pseudopodia. (B) Cell viability of TPC-1/BCPAP cells encapsulated in GelMA:SA = 3:1, 1:1, and 1:3 hydrogels over 3 days measured by CCK-8 assay. (C) Relative mRNA expression of N-cadherin and MMP-9 in cells after culture in the three hydrogel formulations, normalized to the 1:1 group (ns: not significant, $^{**}p < 0.01$)

4. Discussion

As illustrated in Figure 1, the integration of GelMA and calcium alginate allowed the creation of a porous, biocompatible, and mechanically supportive matrix for thyroid cancer cells. This DN hydrogel combines the tunable bioactivity of GelMA with the ionic crosslinking and stability offered by alginate, leading to a platform capable of recapitulating the key features of the tumor extracellular matrix. The porous architecture, highlighted schematically, is critical for supporting cancer cell invasion and migration, as it provides physical pathways and biochemical cues resembling those in native tissues [21]. Notably, such a 3D invasion model enables the study of epithelial–mesenchymal transition (EMT), extracellular matrix degradation, and drug responses under conditions closer to physiological reality than flat cultures [22]. Therefore, this model not only serves as a foundation for mechanistic studies of thyroid cancer progression but also provides a promising tool for evaluating therapeutic strategies in a biomimetic microenvironment.

As illustrated in Figure 2, the GelMA/SA ratio strongly dictates hydrogel performance, and the 1:1 DN composition shows the most desirable overall profile. Excess SA (1:3) confers high swelling capacity but leads to rapid degradation and weak mechanical integrity, making it unsuitable for sustained cell culture. Conversely, GelMA-rich gels (3:1) are structurally stable but exhibit limited swelling, which may reduce nutrient transport and cellular activity. The 1:1 group provides a balanced swelling ratio with moderate degradation, ensuring hydration and structural maintenance during long-term incubation. Importantly, the mechanical analysis was carried out on the 1:1 GelMA/SA hydrogel, which demonstrated pronounced improvements in both tensile and compressive properties compared to the single-component gels. This reflects the synergistic contribution of GelMA's covalent crosslinks and alginate's ionic network. The enhanced strength ensures the hydrogel maintains integrity under deformation and culture stress, which is particularly advantageous for supporting three-dimensional thyroid cancer invasion models. Therefore, the data suggest that the 1:1 GelMA/SA hydrogel is the optimal choice, offering a favorable balance of swelling, degradation, and mechanical performance for biological applications [23,24].

As illustrated in Figure 3, the observed microstructural differences directly explain the functional variations among the hydrogel groups. The SA hydrogel, though hydrophilic and able to swell, forms a mechanically weak matrix due to its soft and easily deformable ionic crosslinks. During dehydration and SEM preparation, this weak framework tends to collapse, which is why only faint or poorly defined pores are observed. Such a structure restricts nutrient diffusion and reduces its ability to support cell

infiltration, consistent with the limited biological activity seen in SA-rich gels. GelMA hydrogels, by contrast, rely on covalent photocrosslinking to form a more stable backbone, which allows the network to maintain larger and more open pores. However, because GelMA alone lacks the additional ionic reinforcement, its pore walls appear thin and less resistant to collapse, leading to structural fragility over extended culture [25]. The DN hydrogel (1:1) integrates these two mechanisms: the GelMA component provides rigidity and shape fidelity, while the SA component contributes ionic crosslinks that distribute stress and prevent wall collapse. As a result, this hybrid structure not only maintains uniform pores but also exhibits thicker and more resilient walls [26]. Such a morphology is particularly advantageous for building three-dimensional thyroid cancer invasion models, as it permits efficient nutrient and oxygen transport while maintaining a robust scaffold for cell adhesion, proliferation, and invasion. Thus, the SEM data strongly support the conclusion that the 1:1 GelMA/SA DN hydrogel achieves an optimal balance between porosity and mechanical stability, making it superior to either single-component system [27].

As illustrated in Figure 4, the biological response of thyroid cancer cells to the hydrogel microenvironment was strongly influenced by the GelMA/SA ratio. The confocal image (Figure 4A) highlights how the intermediate 1:1 hydrogel composition provided a balanced environment, enabling cells to extend pseudopodia and establish strong interactions with the surrounding matrix. This behavior suggests that the porous yet mechanically stable DN scaffold at this ratio can effectively transmit adhesion cues and promote cytoskeletal reorganization. The CCK-8 assay results (Figure 4B) further demonstrate the differential proliferative capacities: while the 3:1 gels promoted higher proliferation, this was associated with a denser matrix that limited spreading, potentially leading to more compact cell clusters rather than invasive morphology. On the other hand, the SA-rich 1:3 gels provided a soft but biologically inert environment, resulting in poor cell proliferation and rounded morphologies [28]. The gene expression data (Figure 4C) reinforce this interpretation. Cells in 1:1 gels retained moderate expression of N-cadherin and MMP-9, indicating the capacity for migration and extracellular matrix remodeling, both of which are essential for invasion studies. The suppression of these genes in the 1:3 group reflects the inability of cells to activate invasive programs in a highly inert network, while the similar expression levels between 1:1 and 3:1 suggest that both environments allow partial maintenance of invasive markers, though with different implications for morphology and viability [23]. Collectively, these findings underscore that the 1:1 hydrogel composition provides the most favorable compromise, supporting both cell viability and functional phenotype, thereby offering the most physiologically relevant platform for constructing thyroid cancer invasion models.

5. Conclusion

In this study, we established a GelMA/SA DN hydrogel system as a three-dimensional platform for modeling thyroid cancer cell invasion. Through systematic evaluation of swelling, degradation, and mechanical properties, we demonstrated that the hydrogel composition critically determines both physicochemical stability and biological performance. SA-rich gels exhibited excessive swelling and rapid degradation, accompanied by poor pore formation and reduced cellular support, while GelMA-rich gels provided mechanical stability but limited porosity and restricted cell spreading. Importantly, the intermediate GelMA:SA = 1:1 formulation achieved a balanced profile, combining adequate swelling with moderate degradation, uniform porous morphology, and enhanced tensile and compressive strength. When thyroid cancer cells (TPC-1/BCPAP) were encapsulated, the 1:1 hydrogel supported well-spread morphology with pseudopodia formation, robust viability, and maintenance of invasion-associated markers such as N-cadherin and MMP-9. These results collectively indicate that the GelMA:SA= 1:1 hydrogel provides the most favorable microenvironment for simulating the invasive behavior of thyroid cancer cells. This work highlights the potential of optimized DN hydrogels to serve as reliable biomimetic scaffolds for cancer biology studies and therapeutic evaluation.

Acknowledgement: Not applicable.

Funding Statement: The study was supported by the Nursing Research Fund Projects of School of Medicine, Shanghai Jiao Tong University (Jyh2206) with Xiao Feng.

Author Contributions: All authors contributed to this present work: Xiao Feng designed the study, Xiaohong Xu acquired the data, Wenqi Tang interpreted the data. Xiao Feng drafted the manuscript, Wenqi Tang revised the manuscript. All authors reviewed and approved the final version of the manuscript.

Availability of Data and Materials: The datasets generated and/or analyzed during the current study are available from the corresponding author Wenqi Tang upon reasonable request.

Ethics Approval: Not applicable.

Conflicts of Interest: The authors declare no conflicts of interest.

Abbreviations

BCPAP	Bonn Cancer Papillary thyroid carcinoma cell line
BSA	Bovine Serum Albumin
CCK-8	Cell Counting Kit-8
cDNA	Complementary Deoxyribonucleic Acid
DAPI	4′,6-Diamidino-2-Phenylindole
DMEM	Dulbecco's Modified Eagle Medium
ECM	Extracellular Matrix
FBS	Fetal Bovine Serum
GelMA	Gelatin Methacryloyl
IF	Immunofluorescence
LAP	Lithium Phenyl-2,4,6-trimethylbenzoylphosphinate
OD	Optical Density
PBS	Phosphate-Buffered Saline
P/S	Penicillin–Streptomycin
qPCR	Quantitative Polymerase Chain Reaction
RNA	Ribonucleic Acid
RT	Room Temperature
SA	Sodium Alginate
SEM	Scanning Electron Microscopy
STR	Short Tandem Repeat
TPC-1	Thyroid Papillary Carcinoma-1 cell line
TRIzol	Total RNA Isolation Reagent
UV	Ultraviolet

References

1. Lee EK, Lee YA. Pediatric thyroid cancer: key considerations based on the 2024 Korean Thyroid Association Differentiated Thyroid Cancer Management Guidelines. Ann Pediatr Endocrinol Metab. 2025;30(1):48–51. doi:10.6065/apem.2448296.148.
2. Medenica S, Arjunan D, Mladenovic V, Zankovic N, Aksam S, Gluvic Z, et al. Thyroid nodules and thyroid cancer in pregnancy. Gynecol Endocrinol. 2025;41(1):2517878. doi:10.1080/09513590.2025.2517878.
3. Tang L, Angell TE. Thyroid cancer. Semin Perinatol. 2025;49(2):152042. doi:10.1016/j.semperi.2025.152042.

4. Meng W, Huang Q, Zhang R, Shen J, Xie D, Xu C, et al. Protocol for analyzing invadopodia formation and gelatin degradation. STAR Protoc. 2024;5(4):103399. doi:10.1016/j.xpro.2024.103399.
5. Pishdad R, Barbesino G, Wirth LJ. Familial thyroid cancers syndromes. Endocrinol Metab Clin N Am. 2025;54(3):521–36. doi:10.1016/j.ecl.2025.03.018.
6. Miao F, Liu T, Zhang X, Wang X, Wei Y, Hu Y, et al. Engineered bone tissues using biomineralized gelatin methacryloyl/sodium alginate hydrogels. J Biomater Sci Polym Ed. 2022;33(2):137–54. doi:10.1080/09205063.2021.1980360.
7. Li H, Chen S, Dissanayaka WL, Wang M. Gelatin methacryloyl/sodium alginate/cellulose nanocrystal inks and 3D printing for dental tissue engineering applications. ACS Omega. 2024;9(49):48361–73. doi:10.1021/acsomega.4c06458.
8. Kong Y, Tang H, Chai H, Zhang L, Mao Z, Xu H. Asymmetric adhesive and absorbable fiber membrane of methacrylated gelatin-gelatin/acetylcysteine for advanced hemostatic applications. ACS Appl Polym Mater. 2025;7(13):8383–95. doi:10.1021/acsapm.5c00548.
9. Hickman JA, Graeser R, De Hoogt R, Vidic S, Brito C, Gutekunst M, et al. Three-dimensional models of cancer for pharmacology and cancer cell biology: capturing tumor complexity *in vitro*/*ex vivo*. Biotechnol J. 2014;9(9):1115–28. doi:10.1002/biot.201300492.
10. Fang H, Xu J, Ma H, Feng Z, Cheng YY, Nie Y, et al. A quercetin nanoparticle combined with a 3D-printed decellularized extracellular matrix/gelatin methacryloyl/sodium alginate biomimetic tumor model for the treatment of melanoma. Int J Biol Macromol. 2025;288:138680. doi:10.1016/j.ijbiomac.2024.138680.
11. Usman M, Mac Regenstein J, Rahman HUU, Ishaq A, Khan MI, Sahar A, et al. Structural and functional characterization of *Coryphaena hippurus* skin gelatin with commercial porcine gelatin. Appl Food Res. 2025;5(1):100898. doi:10.1016/j.afres.2025.100898.
12. Izgordu MS, Ayran M, Ulag S, Yildirim R, Bulut B, Sahin A, et al. Fabrication of gentamicin sulfate-loaded 3D-printed polyvinyl alcohol/sodium alginate/gelatin-methacryloyl hybrid scaffolds for skin tissue replacement. Macromol Mater Eng. 2023;308(12):2300151. doi:10.1002/mame.202300151.
13. Matinong AME, Pickering KL, Waterland MR, Chisti Y, Haverkamp RG. Gelatin and collagen from sheepskin. Polymers. 2024;16(11):1563. doi:10.3390/polym16111563.
14. Gaidau C, Râpă M, Ionita G, Stanculescu IR, Zaharescu T, Constantinescu RR, et al. The influence of gamma radiation on different gelatin nanofibers and gelatins. Gels. 2024;10(4):226. doi:10.3390/gels10040226.
15. Behrouznejad B, Sadat SB, Masaeli E. Impact of diverse gelatin-included culture media on fabricated bacterial cellulose/gelatin hydrogel properties: a holistic exploration. Int J Biol Macromol. 2025;322(Pt 2):145842. doi:10.1016/j.ijbiomac.2025.145842.
16. Cao H, Wang J, Hao Z, Zhao D. Gelatin-based biomaterials and gelatin as an additive for chronic wound repair. Front Pharmacol. 2024;15:1398939. doi:10.3389/fphar.2024.1398939.
17. Calixto S, Alfaro-Gomez M. Dichromated gelatin in optics. Gels. 2025;11(4):298. doi:10.3390/gels11040298.
18. Jang Y, Jang J, Kim BY, Song YS, Lee DY. Effect of gelatin content on degradation behavior of PLLA/gelatin hybrid membranes. Tissue Eng Regen Med. 2024;21(4):557–69. doi:10.1007/s13770-024-00626-4.
19. Kheradvar Kolour A, Ghoraishizadeh S, Zaman MS, Alemzade A, Banavand M, Esmaeili J, et al. Janus films wound dressing comprising electrospun gelatin/PCL nanofibers and gelatin/honey/curcumin thawed layer. ACS Appl Bio Mater. 2024;7(12):8642–55. doi:10.1021/acsabm.4c01449.

20. Farasatkia A, Kharaziha M. Robust and double-layer micro-patterned bioadhesive based on silk nanofibril/GelMA-alginate for stroma tissue engineering. Int J Biol Macromol. 2021;183:1013–25. doi:10.1016/j.ijbiomac.2021.05.048.
21. Tobo C, Jain A, Gamage ME, Jelliss P, Garg K. Electrostatic gelatin nanoparticles for biotherapeutic delivery. Gels. 2024;10(12):757. doi:10.3390/gels10120757.
22. Liu X, Shu Y, Zhu J, Fang H, Su Y, Ma H, et al. A 3D bioprinted potential colorectal tumor model based on decellularized matrix/gelatin methacryloyl/nanoclay/sodium alginate hydrogel. Int J Biol Macromol. 2025;293(1):139346. doi:10.1016/j.ijbiomac.2024.139346.
23. Liu Y, Zheng F, Zhao H, Li J, Dong D, Yuan C, et al. Physicochemical and digestible properties of corn starch/gelatin complexes: effect of pH, type of gelatin, and gelatin/starch ratio. Food Hydrocoll. 2024;156:110268. doi:10.1016/j.foodhyd.2024.110268.
24. Yildiz ZI, Topuz F, Kilic ME, Durgun E, Uyar T. Gelatin-based and gelatin-free electrospun fibers of lycopene/cyclodextrin inclusion complexes with potent antioxidant activity. ACS Food Sci Technol. 2024;4(4):833–41. doi:10.1021/acsfoodscitech.3c00497.
25. Wang N, Floriano Marcelino T, Ade C, Pendlmayr S, Ramos Docampo MA, Städler B. Collagenase motors in gelatine-based hydrogels. Nanoscale. 2024;16(20):9935–43. doi:10.1039/d3nr05712g.
26. Wang S, Han Q, Zhang D, Liu J, Shen Z, Wei X, et al. Development and characterization of carboxymethyl chitosan/sodium alginate/gelatin methacryloyl hydrogels as wound dressing materials. Mat Express. 2022;12(12):1572–6. doi:10.1166/mex.2022.2301.
27. Ma C, Kim YK, Lee MH, Jang YS. Development of gelatin methacryloyl/sodium alginate interpenetrating polymer network hydrogels for bone regeneration by activating the Wnt/β-catenin signaling pathway via lithium release. Int J Mol Sci. 2023;24(17):13613. doi:10.3390/ijms241713613.
28. Silverthorne KEC, Donahue-Boyle EM, Pricu A, Li AY, Brook MA. Biodegradable, crosslinked silicone-gelatin hydrogels. Green Chem. 2024;26(10):6200–8. doi:10.1039/d4gc00402g.

Received: 19 September 2025; Accepted: 11 March 2026; Published: 29 June 2026